Low Temperature Physics/Fizika Nizkikh Temperatur, 2015, v. 41, No. 9, pp. 864–877

Spin waves damping in nanometre-scale magnetic materials

(Review Article)

V.N. Krivoruchko

Donetsk Institute for Physics and Engineering, the National Academy of Sciences of Ukraine
46 Nauki Ave., Kyiv 03680, Ukraine
E-mail: krivoruc@gmail.com

Received March 23, 2015, published online July 24, 2015

Spin dynamics in magnetic nanostructured materials is a topic of great current interest. To describe spin motions in such magnetic systems, the phenomenological Landau–Lifshitz (LL), or the LL–Gilbert (LLG), equation is widely used. Damping term is one of the dominant features of magnetization dynamics and plays an essential role in these equations of motion. The form of this term is simple; however, an important question arises whether it provides a proper description of the magnetization coupling to the thermal bath and the related magnetic fluctuations in the real nanometre-scale magnetic materials. It is now generally accepted that for nanostructured systems the damping term in the LL (LLG) equation fails to account for the systematics of the magnetization relaxation, even at the linear response level. In ultrathin films and nanostructured magnets particular relaxation mechanisms arise, extrinsic and intrinsic, which are relevant at nanometre-length scales, yet are not so efficient in bulk materials. These mechanisms of relaxation are crucial for understanding the magnetization dynamics that results in a linewidth dependence on the nanomagnet's size. We give an overview of recent efforts regarding the description of spin waves damping in nanostructured magnetic materials. Three types of systems are reviewed: ultrathin and exchange-based films, magnetic nanometre-scale samples and patterned magnetic structures. The former is an example of a rare case where consideration can be done analytically on microscopic footing. The latter two are typical samples when analytical approaches hardly have to be developed and numerical calculations are more fruitful. Progress in simulations of magnetization dynamics in nanometre-scale magnets gives hopes that a phenomenological approach can provide us with a realistic description of spin motions in expanding diverse of magnetic nanostructures.

PACS: **75.75.–c** Magnetic properties of nanostructures;
75.78.–n Magnetization dynamics;
75.30.Ds Spin waves.

Keywords: magnetic nanostructures and nanoelements, magnetization dynamics, Gilbert damping, spin wave relaxation mechanisms.

Contents

1. Introduction, background equations 865
2. Ultrathin and exchange-based films 866
2.1. Two-magnon scattering 866
2.2. Nonlocal relaxation 868
2.3. Unidirectional damping 869
3. Damping in magnetic nanometre-scale samples 869
3.1. Three-magnon scattering 870
3.2. Longitudinal relaxation 871
3.3. Anisotropic damping in nanoelements 872
4. Nanometre-scale patterned magnetic structures 873
4.1. FMR damping 873
4.2. Spin waves anisotropic propagation and damping 874
5. Conclusion 875
References 876

© V.N. Krivoruchko, 2015

1. Introduction, background equations

In 1935, Landau and Lifshitz [1] proposed the equation for the dynamics of the magnetization **M** of a uniform ferromagnet in an effective field $\mathbf{H}_{\text{eff}}$ of the form:

$$\partial \mathbf{M} / \partial t = -\gamma \mathbf{M} \times \mathbf{H}_{\text{eff}} - \gamma \frac{\alpha}{M_s} [\mathbf{M} \times (\mathbf{M} \times \mathbf{H}_{\text{eff}})] \ , \quad (1)$$

where γ is the absolute value of gyromagnetic ratio, t is time, M_s stands for the saturation magnetization, and α is the damping constant. The first term in Landau–Lifshitz (LL) equation describes the precession of the magnetization around the micromagnetic effective field $\mathbf{H}_{\text{eff}}$, which is composed of the external magnetic field, the magnetic anisotropy field, the demagnetization field, etc. In the absence of damping, this leads to the Larmor precession with a well-defined frequency, ω. In all real systems, there are different "friction" processes that cause precession damping. The second term is phenomenological representation of one or more (unspecified) energy loss mechanisms. It breaks the time-inversion symmetry and consequently leads to the precession damping. This term drives the magnetization toward the direction of $\mathbf{H}_{\text{eff}}$, whereby angular momentum is transferred to nonmagnetic degrees of freedom (direct damping). Good samples in ferromagnetic resonance satisfy $\alpha << 1$.

In the 1955 MMM conference proceedings, Gilbert argued that the LL damping fails for large enough damping [2]. Instead, he proposed an expression that, for a small angle between $\mathbf{H}_{\text{eff}}$ and **M**, may be written as follows:

$$\partial \mathbf{M} / \partial t = -\gamma_G \mathbf{M} \times \mathbf{H}_{\text{eff}} + \frac{\lambda}{M_s} (\mathbf{M} \times \partial \mathbf{M} / \partial t) \ . \quad (2)$$

As for Eq. (1), the second term in the r.h.s. of the LL–Gilbert (LLG) equation is a damping term introduced in a phenomenological manner. It is instructive to rewrite Eq. (2) in the form

$$\partial \mathbf{M} / \partial t = -\gamma_G \mathbf{M} \times \left(\mathbf{H}_{\text{eff}} - \frac{\lambda}{\gamma_G M_s} \partial \mathbf{M} / \partial t \right) .$$

Clearly, we obtain an attractive interpretation that the damping introduces an effective magnetic field opposite in direction to $\mathbf{H}_{\text{eff}}$ and proportional to $\partial\mathbf{M}/\partial$t. With $\lambda = \alpha$ and $\gamma_G = \gamma (1 + \lambda^2 / M_s^2)$, the LL and the Gilbert forms are mathematically equivalent. Yet, this equivalency (within a linear approximation) is only for small damping and low enough microwave frequency f (or $\omega = 2\pi f$ the angular frequency). Indeed, for example, in the parallel ferromagnetic resonance (FMR) configuration, with the magnetization parallel to the applied field, the time derivative $\partial\mathbf{M}/\partial t$ Gilbert term in the equation of motion produces a FMR linewidth linear with the frequency f, in contrast to the LL equation.

Damping is measured through the linewidth ΔH of the absorption peak in the transverse susceptibility spectrum. In a conventional fixed frequency field-swept FMR experiment, when the magnetization is aligned with either an in-plane or perpendicular to the plane applied magnetic field, the absorption linewidth (full width at half maximum) is given by $\Delta H = 4\pi\lambda M_s f / \gamma$ i.e., the linewidth in these cases is proportional to the frequency with a slope determined by λ. This is the homogeneous or *intrinsic* contribution to the FMR linewidth. However, in many magnetic systems, while a linear behavior is observed, the linewidth fails to extrapolate to zero with vanishing frequency. Experiments show an additional frequency-independent contribution to the linewidth:

$$\Delta H = \Delta H_0 + 4\pi\lambda M_s f / \gamma \ .$$

Here zero-frequency contribution to the linewidth ΔH_0 is related to an *extrinsic* mechanism and reflects the effect of inhomogeneity on the linewidth. Thus, frequency dependent studies allow distinguishing intrinsic and extrinsic contributions to the relaxation.

Both the LL and the LLG equations were introduced with suggestion that (i) magnetization motion is small, (ii) the damping parameter is isotropic, and, in ferromagnets, (iii) it is assumed that the length of the magnetization is conserved locally (|**M**| = const) as it relaxes to its equilibrium position. These restrictions are caused by the structure of the damping term. It is also assumed that α (or λ) is independent on effective field $\mathbf{H}_{\text{eff}}$. Concerning the last assumption, Callen was the first who pointed out that the constant α is the result of a small angle expansion θ (θ represents the angle between the magnetization vector and $\mathbf{H}_{\text{eff}}$) [3]. Keeping next-to-leading-order terms, he predicted that $\alpha \sim [1 - \cos\theta] / \sin^2\theta$, which is sufficient to stabilize a precessing spin-wave mode at larger θ.

A large body of both experimental and theoretical work confirmed that the magnetization dynamics of a *bulk* ferromagnet is well described by the phenomenological equations (1) or (2), and the damping mechanism in bulk ferromagnets is relatively well understood at present. Yet, we note here that, even for the bulk systems, as Bar'yakhtar pointed out [4], the form of the second term in Eq. (1) is very restrictive. Its structure assumes that the equation of motion is form invariant under arbitrary rotations of the coordinate system, whereas in any ferromagnet the equation only needs to be form invariant under rotations about the axis along the magnetization direction (in the presence of anisotropy, the symmetry is lower). Thus, symmetry allows for a generalized form of the damping term on the r.h.s. of Eq. (1) (see textbook [5] for more details).

At present, the static and dynamic properties of nanostructured magnetic materials are among the most active research topics in magnetism. This is, in particular, due to the promising prospects for application of such materials within magnetic data storage [6], magnonic devices [7]

(the magnetic counterpart of a photonic crystal), as spin-wave filters [8], etc. Recently, a multidisciplinary branch of science called “magnonics” developed as a result of activity is this field [9]. It focuses on studies of spin waves, and more generally on magnetic excitations, in artificial materials with periodic variations of magnetic properties — magnonic crystals. Magnonics is strongly coupled to material science since it requires materials with small magnetic damping. The main obstacle in the field of magnonics is still the spin-wave relaxation, which has to be decreased utilizing new materials or to be compensated using new energy-efficient means. Magnetoelectronics is another region of application [10]. As demonstrated by Slonczewski [11] and Berger [12] the interaction between localized magnetic moments and conducting electrons leads to the so-called spin transfer torque, which accounts for the ability of a spin-polarized current to interact with the magnetization of a ferromagnetic layer via transfer of the spin angular momentum. Such a current-induced spin transfer enables the manipulation of magnetic nanodevices. Yet, this “pumping” of spins also slows down the magnetization precession corresponding to an enhanced Gilbert damping constant in the LL equation [13]. The damping parameter is also a critical figure for the efficient operation of magnetoelectronic devices.

In device design the LL or the LLG equations are widely used to describe spin motions in magnetic nanoscale structures. An important question is whether it provides a proper description of the damping of the magnetization in real nanoscale materials or not. Indeed, as follows from the experiment, the situation is more complex if we deal with the magnetization dynamics in thin magnetic films and nanostructured magnets. For example, the damping constant was found to be $0.04 < \alpha < 0.22$ for Cu–Co and Pt–Co in thin film pillars [14], which is considerably larger than the bulk value $\alpha \approx 0.005$ in Co [15] or $\alpha \approx 0.004$ for thin film Permalloy [16]. Recent works on magnetic nanostructures demonstrate a strong dependence of the effective damping on the nanomagnet size and the particular spin-wave mode [17,18]. It is important to understand how scaling effects damping and linewidth.

It is now widely accepted that the mechanisms usually applied to describe the spin waves damping in bulk magnetic systems cannot explain the experimental data obtained on ultrathin films and nanostructured magnetic materials. Possible novel mechanisms of spin waves damping in such systems were predicted and are under extensive discussion at present. In this report, the questions concerning the magnetization relaxation in nanostructured magnetic materials have been reviewed. Naturally, in this intensively expanding research field, we are forced to restrict ourselves to some narrow area. The mechanisms for magnetization damping in heterostructures of ferromagnet and normal conductors are beyond the scope of this report, for a review on this topic see, e.g., Ref. 10. In this paper, we do not touch upon the question of the LL (LLG) equations and the magnetization damping generalization for fast (on the time scale of about 100 fs) magnetization dynamics. A recent review concerning ultrafast dynamics and the optical manipulation of magnetic order can be found in Refs. 19–21. We will concentrate here mainly on three types of interesting systems: (i) ultrathin and exchange-based films, (ii) magnetic nanometre-scale samples, and (iii) patterned magnetic structures. Ultrathin films is a rare example when theoretical consideration can be done analytically on microscopic footing. The nano-scale magnets and patterned magnetic structures are systems modelling of which can be hardly developed analytically, and numerical calculations based on the generalized LL (LLG) equations are typically used. Specific of nanometre-scale samples is originated by their finite format and the fact that, due to the highly inhomogeneous internal magnetic field within the nanoelement, their magnetic resonances may exhibit strong spatial localization, so that the resonance spectra are discrete. Concerning patterned magnetic systems, their properties are a nontrivial combination of those of thin film and nanoelement. Some features here we illustrate on the example of thin film with mesh of holes (antidots).

2. Ultrathin and exchange-based films

It is now generally accepted that for ultrathin and exchange-based films specific relaxation processes arise, which operate at small-length scales, and which are not relevant for bulk materials. These processes conventionally are parted into two classes, intrinsic and extrinsic, and both are crucial for understanding the magnetization dynamics. The intrinsic processes have been well known and (conventionally) summarized as Gilbert damping [22]; the key role of the extrinsic relaxation processes has been understood and analyzed in detail most recently. Their significance arises because of the fact that a large fraction of the magnetic moments are in or near surfaces and interfaces. We illustrate the specific role of the surface in nanostructured magnets on the example of ultrathin and exchange-based films.

2.1. Two-magnon scattering

Two-magnon damping in ultrathin films and different layered structures was proposed in Ref. 23 and is based on two magnon scattering processes induced by defects or, in general, magnetic inhomogeneity. The inhomogeneity contribution is associated with disorder and their effect is at least twofold. First, fluctuations in the materials magnetic properties such as its anisotropy or magnetization lead to a linewidth that is frequency independent. In a simple picture, independent parts of the sample come into resonance at different applied magnetic fields. Second, disorder can couple the uniform precessional mode with k equals zero, excited in an FMR experiment, to degenerate finite-k spin-

wave modes. This mechanism of relaxation of the uniform mode, known as two-magnon scattering [22], requires a spin-wave dispersion with finite-k modes that are degenerate with zero-k mode, which only occurs for certain magnetization orientations. Let us briefly remind the main ideas of this field (for more details see, e.g., textbook [22]).

Following [24], the scattering of a magnon with wave vector k_1 into another magnon k_2 by a process that does not conserve momentum is described by the Hamiltonian:

$$H_{sc} = \sum_{k_1,k_2} V(k_1,k_2)(a^+_{\mathbf{k}_1} a_{\mathbf{k}_2} + \text{h.c.}) \ , \qquad (3)$$

where $a^+_{\mathbf{k}}$ and $a_{\mathbf{k}}$ are the creation and annihilation magnon operators and $V(k_1,k_2)$ represents the scattering perturbation. For an ideal (strictly periodic) crystal $V(k_1,k_2) = 0$ if $k_1 \neq k_2$ due to impulse conservation law. Yet, if the crystal (film) is imperfect $V(k_1,k_2) \neq 0$.

Consider relaxation of a spin wave with wave vector $\mathbf{k}_1$. Within simple perturbation-theory calculation, the magnon number $n_{\mathbf{k}_1}$ rate of change is

$$\frac{dn_{k_1}}{dt} = \frac{2\pi}{\hbar}\sum_{k_2} |V(k_1,k_2)|^2 \ (n_{\mathbf{k}_2} - n_{\mathbf{k}_1})\delta(\hbar\omega_{k_1} - \hbar\omega_{k_2}) \ . \ (4)$$

Thus, standard transition probability calculation yields for the two-magnon contribution to the linewidth

$$\Delta H^{(2)} = \frac{\pi}{\hbar}\sum_{k_2} |V(k_1,k_2)|^2 \ \delta(\hbar\omega_{k_1} - \hbar\omega_{k_2}) \ . \qquad (5)$$

This expression implies that incoming magnon $\mathbf{k}_1$ relaxes by scattering into all degenerate modes with wave vector $\mathbf{k}_2$. If $\mathbf{k}_1 = 0$, i.e., we deal with homogeneous magnetization precession, these processes called a 0-k processes of relaxation. The remaining task is for a given sample to model the surface and/or interface defects, and to find their contribution to the matrix elements $V(k_1,k_2)$.

Usually, the two-magnon scattering is less important in bulk ferromagnet, but is of particular importance in magnetic nanostructures because real magnetic superlattices and ultrathin films have steps and defects on a length scale of some hundreds of nanometres. This is the order of magnitude for long wavelength magnons, into which the uniform motion of magnetization can scatter. Following Mills *et al.* [23], consider an in-plane magnetized film. The FMR frequency ω_{FMR} of an ideal ultrathin film equals that $\omega_{\mathbf{k}}$ of a spin wave with wave vector $\mathbf{k}$ equals zero. As is known, in a thin ferromagnet film and at long wavelengths, dipolar couplings produce terms in $\omega_{\mathbf{k}}$ linear in $|\mathbf{k}|$. The initial slope of $\omega_{\mathbf{k}}$ depends on the angle φ between $\mathbf{k}$ and the magnetization $\mathbf{M}_S$, assumed in the plane. If $|\varphi| < \varphi_c(H_0)$, or if $|\pi - \varphi| < \varphi_c(H_0)$, then this initial slope is negative. Here $\sin(\varphi_c(H_0)) = (H_0/[B_0 + H_S])^{1/2}$, where H_0 is magnetic field applied parallel to M_S, $B_0 = H_0 + 4\pi M_S$, and H_S is the surface anisotropy field taken positive when the surface normal is a hard axis. Exchange contributes to $\omega_{\mathbf{k}}$ term proportional to Dk^2, with D being the exchange stiffness.

Thus, for $|\varphi| < \varphi_c(H_0)$ and also $|\pi - \varphi| < \varphi_c(H_0)$ we have spin waves of wave vector $\mathbf{k}_c(\varphi)$ degenerate with the FMR mode, as illustrated in Fig. 1. Static defects such as surface imperfections scatter energy from the FMR mode to the finite wave vector modes of the same frequency, to relax the FMR mode by a dephasing process. This is, for the ultrathin film, a direct analog of the relaxation mechanism discussed many years ago [24]. Associated with such scatterings is necessarily a shift in frequency of the FMR mode.

The authors [23] modelled surface defects as rectangular islands and argued that the dominant contribution to the two-magnon matrix element has its origin, for typical samples, in the perturbation of the surface anisotropy field near the islands. Under the conditions specified in Ref. 23 and usually realized in experiments, this theory provides that the extrinsic linewidth can be written as follows:

$$\Delta H^{(2)} \propto \arcsin\left\{\frac{\left[(\omega_0/2)^{1/2} + \omega^2_{FMR}\right]^{1/2} - \omega_0/2}{\left[(\omega_0/2)^{1/2} + \omega^2_{FMR}\right]^{1/2} + \omega_0/2}\right\}^{1/2} , \ (6)$$

where, $\omega_0 = \gamma(4\pi M_S + H_S)$. If $\omega_0 >> \omega_{FMR}$, then Eq. (6) predicts that the linewidth should vary linearly with frequency, very much as the prediction of the LLG equation. However, under typical conditions $\omega_{FMR} \sim \omega_0$ and in this regime Eq. (6) yields strong deviations from linear behavior. For experimentally accessible FMR frequencies, analysis of Eq. (6) shows that the linewidth increases with frequency much slower than expected from the linear law. This means, in particular, that the damping term is nonlocal in time. A general consequence is that the linear frequency dependence predicted from the LLG phenomenology is qualitatively incorrect for the real materials.

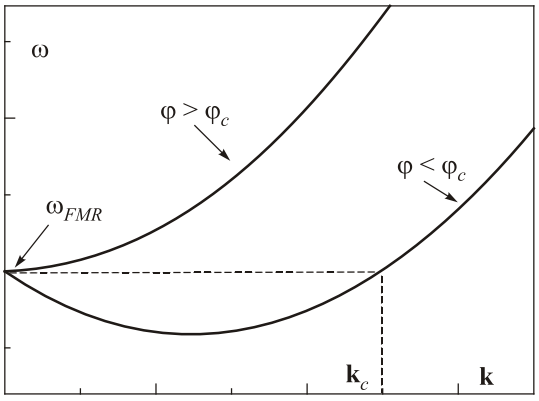

Fig. 1. A schematic illustration of the spin wave dispersion with two angles of propagation, one is less than the critical angle φ_c and another is larger, for in-plane magnetized film.

Resonance experiments [25] on magnetic multilayer nanostructures in a frequency range of more than two orders of magnitude show an unambiguous nonlinear frequency dependence of the linewidth $\Delta H^{(2)}(\omega)$. It was found that two-magnon scattering is not effective in FMR when applied field is perpendicular to the film plane, but may be very important for various directions of the external field applied in the film plane. The viscous Gilbert damping and two-magnon scattering were clearly separated. Analysis of angular and frequency dependent measurements has shown that a transverse scattering within the magnetic subsystem is a main mechanism of relaxation. The longitudinal relaxation into the thermal bath, when the length of the magnetization vector does not conserve $|\mathbf{M}| \neq$ const (see subsection 3.2, below), is up to two orders of magnitude smaller.

In the presence of a periodic scattering potential the spin relaxation in ultrathin ferromagnets is not a monotonous function of the frequency, as has been usually assumed. In report [26], a phenomenological theory of the two-magnon scattering in periodically structured thin-film systems was developed. The authors demonstrate that the frequency dependence of the overall spin relaxation in a large class of ferromagnetic systems is not monotonous and depends on the defect structure. In particular, the spin relaxation rate is found to increase substantially at characteristic frequencies related to the periodicity of the magnon scattering potential. Consequently, the usual practice of separation of intrinsic and extrinsic spin relaxation processes by means of their frequency dependence, strictly speaking, must be reconsidered. The exact structure of defects in a material, being periodic in the majority of ferromagnetic systems, needs to be cleared up first.

Damping of spin waves in magnonic crystals was analyzed in reports [27]. Authors obtained an analytical expression for the effective damping coefficient of propagating spin waves as function of system parameters and shown, in particular, that it strongly depends on the spin wave frequency and bias magnetic field. This dependence is more pronounces when damping is localized in the vicinity of interface. Thus, the effective damping coefficient can be designed by means of a proper choice of the depth modulation of magnetic parameters.

These results are important for future developments, since they could explain the anomalous spin relaxation in magnonic crystals and help to tailor spin relaxation in spintronic devices by artificially inducing a defect structure to activate a desired spin relaxation channel in a specific frequency range.

2.2. Nonlocal relaxation

The FMR linewidth is related to the relaxation rate of the magnon with zero wave number **k**. In order to obtain more information on the magnon relaxation, in Ref. 28 investigated the behavior of magnons with $\mathbf{k} \neq 0$, which can be measured with Brillouin light scattering (BLS). It was found that the damping increases strongly with the wave vector. This means that damping term is nonlocal in space. That is another example of a damping mechanism not present in bulk materials yet operating in ultrathin ferromagnets.

Both the FMR and BLS linewidth data are consistently explained by a relaxation mechanism based on two-magnon scattering processes due to the local fluctuation of the exchange coupling caused by interface roughness. As already mentioned, standard calculation of the transition probability yields for the magnon's energy relaxation expression (5). This expression suggests that the incoming magnon $\mathbf{k}_1$ relaxes by scattering into all degenerate modes with wave vector $\mathbf{k}_2$. Authors [28] considered a simple model of exchange-based FM/AFM films where the roughness gives rise to a large fluctuating field because the FM magnetization interacts alternatively with one or the other AFM (antiferromagnetic) sublattice via the atomic exchange coupling. Defects on the FM–AMF interface result in a local perturbation of the exchange coupling with energy $2J_{\text{int}}\cos(\theta)$ per unit area, where J_{int} represents the local interfacial exchange energy and θ is the angle between the FM and AFM moments. Then it can be shown that the strength of the scattering perturbation is [28]:

$$V(k_1,k_2)=\gamma^2\hbar\frac{H_{\text{int}}}{\omega_k}\frac{A_d}{2A}\left[H_x(k_1)+H_y(k_1)\right]S(k_1-k_2)\cos\theta\,. \tag{7}$$

Here $H_{\text{int}} = J_{\text{int}}/M_s d$ stands for the local exchange coupling field (d is the film thickness), A_d and A are the defect and the film area, respectively, $S(k_1 - k_2)$ is a structure factor for the defects,

$$H_x(k)=H\cos(\theta-\theta_H)+2\pi M_s kd\sin^2(\theta_k)+Dk^2+H_a\cos(\theta),$$

$$H_y(k)=H\cos(\theta-\theta_H)+4\pi M_s(1-kd/2)+Dk^2+H_a\cos(\theta),$$

and the frequency of the **k** magnon $\omega_{\mathbf{k}}$ is $\omega_{\mathbf{k}}=\gamma[H_x(k)H_y(k)]^{1/2}$. Here H is the external field applied in the film plane at an angle θ_H with the direction of the unidirectional anisotropy field H_a, θ_k is the angle of the magnon wave vector in the plane, and D is the exchange stiffness of the FM film. Under the conditions usually realized in experiments, the model [28] predicts that both FMR and BLS linewidths vary with the interface energy as J_{int}^2 and with film thickness as $1/d^2$. In addition, the BLS linewidth is inversely proportional to the magnon frequency.

The thickness dependence of the two-magnon model, with an explicit $\sim 1/d^2$ dependence in the scattering strength and a $\sim 1/d$ thickness dependence in the mode counting, does not agree well with the published experimental results [29], which show the linewidth increasing linearly with $1/d$ for $d > 10$ nm and decreasing for a thinner sample. The $1/d^2$ dependence of the scattering strength can be eliminated if the perturbing field is assumed to act on

spins throughout the thickness of the sample, rather than on the surface spins.

A further generalization of this aspect of magnetization dynamics is the implementation of nonlocal effects in both space and time [30]. This can be achieved by introducing a retardation kernel, which takes into account temporal retardation within a characteristic time τ and spatial one with a characteristic scale ζ. The latter simulates an additional mutual interaction of the magnetic moments in different areas of the film within the retardation length ζ. For estimation, the size of inhomogeneity or defect on the film surface may be considered as the length ζ. As for the feedback time, the authors [30] presented arguments why it is reasonable to consider the τ in the interval 0 fs < τ < 100 fs. This time-scale is relevant for ultrafast dynamics.

The nonlocal damping becomes significant when the wavelength of magnons approaches the exchange length of the material, i.e., for high-order exchange dominated spin waves. In report [31], exchange attenuation of standing spin waves is calculated for an ultrathin ferromagnetic film of the order of exchange length thick. It is shown that the wave vectors of standing spin waves in such film achieve values that are proportional to the inverse film thickness. The nonlocal exchange attenuation at such wave vectors becomes dominant and can result in smearing of the standing spin wave spectrum.

Thus, the nonlocal feedback in ferromagnetic resonance leads to linewidth broadening and consequently to spin damping. Whether the magnitude of retardation is able to exceed the Gilbert damping depends strongly on the frequency. In particular, the calculations [30] suggest that, for sufficiently high frequencies, retardation effects dominate the intrinsic damping.

2.3. Unidirectional damping

Recently it was demonstrated experimentally that damping in exchange-coupled systems is not only anisotropic but also unidirectional [32]. This was evidenced by an asymmetry in the damping by inversion of the magnetic field polarity. The study reveals that this asymmetry in the damping is enhanced by the increase in the exchange bias field. It was shown unambiguously that the anisotropy in the intrinsic Gilbert damping originates from the pinned spins of the bilayers and is proportional to the exchange-coupling field $\mathbf{H}_{\text{ex}}$ between bilayers.

To reproduce the experimental features of the resonance absorption, a modified relaxation term in the LLG equation of motion (2) was proposed [32]:

$$\partial\mathbf{M}/\partial t = -\gamma_G \mathbf{M}\times\mathbf{H}_{\text{eff}} + \lambda\left(1-\xi\cos\left(\theta_{\mathbf{H}_{\text{ex}}\mathbf{M}}\right)\right)\mathbf{M}\times\partial\mathbf{M}/\partial t. \quad (8)$$

The term $\sim \xi$ represents the anisotropic damping that depends on the angle $\theta_{\mathbf{H}_{ex}\mathbf{M}}$ between the direction of the magnetization $\mathbf{M}$ holed by an antiferromagnetic layer and the coupling field $\mathbf{H}_{\text{ex}}$. For the samples NiO(67.5nm)/$Ni_{81}Fe_{19}$ the fit to the experimental data gives for $\xi = 0.18$. It was also demonstrated that the value of ξ depends on the thickness of the antiferromagnetic layer. Below the critical thickness ξ is zero, i.e., the relaxation parameter remains unchanged by inversion of the polarity. However, ξ increases with $\mathbf{H}_{\text{ex}}$.

Note that this relation Steiauf and Fähnle [33] used earlier in a phenomenological extension of the *ab initio* density-functional electron theory to derive an equation of motion for the spin dynamics in magnets. The most important result of their calculations is that the magnetization dynamics with a scalar damping term of the Gilbert's form does not depend on the orientation of $\mathbf{M}$ and is valid only for a few specific situations. Even for the case of a homogeneous magnetization, the damping term has to be replaced by a more general term of the form $1/M_S(\mathbf{M}\times\hat{\alpha}(\mathbf{M})\partial\mathbf{M}/\partial t)$ with a damping matrix $\hat{\alpha}(\mathbf{M})$, which depends on the orientation of the magnetization. The orientation dependence of $\hat{\alpha}(\mathbf{M})$ is already substantial in some bulk materials (e.g., in hexagonal *Co*), and it is very strong for systems with reduced dimensionality like monatomic layers or monatomic wires. The authors demonstrate that in the systems with reduced dimensionality there are orientations for which the damping is identically zero and other orientations for which the damping is very large. It was also argued that in the presence of spin-orbit interaction the damping parameter would depend on the direction of the magnetization, too. Thus, the spin-orbit coupling makes the spin degree of freedom respond to its orbital environment.

Safonov [34] has also introduced *ad hoc* a matrix form of magnetization damping for small magnetization motions. The damping tensor is scaled by only one phenomenological damping parameter, which can be obtained from the experiment.

3. Damping in magnetic nanometre-scale samples

An important specific of nanosized samples stems from their finite size and the fact that, even in an ellipsoidal element, their magnetization distribution can be nonuniform and, thus, the internal magnetic field can be inhomogeneous. The magnetic structure shown in Fig. 2 illustrates a possible metastable remanent state — two magnetic vortexes of opposite chirality — that can be realized in nanometer samples subjected to rapidly pulsed magnetic field [35]. Inhomogeneous internal magnetic field $\mathbf{H}_{\text{eff}}$ plays a dominant role in the effective pinning of the dynamic magnetization and induces inhomogeneous magnetization configurations that form a potential wall for spin waves [36,37]. Due to the highly inhomogeneous internal magnetic field within the nanometre-scale sample, its magnetic resonances may exhibit strong spatial localization so that the resonance spectra are discrete [37]. As a result, intrinsic nonlocal effects, moderated by spin-wave mode con-

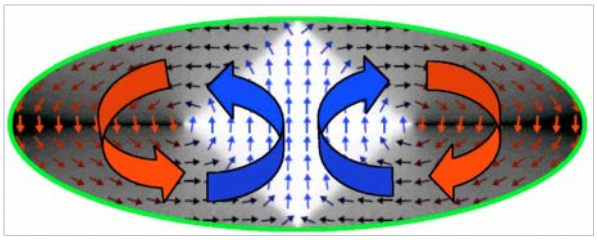

Fig. 2. (Color online) A possible magnetic structure, two magnetic vortex of opposite chirality, which can be realized in nanometer samples under the effect of pulsed field. (Borrowed from [35]).

finement, are important contributors to damping in magnetic nanostructures.

Time-resolved scanning Kerr microscopy investigation of magnetization dynamics of arrays of nonellipsoidal nanomagnets of different sizes directly confirms these conclusions [38]. In the experimental spectra acquired from an element of length of 236 nm and thickness of 13.6 nm, two branches of excited modes were observed to coexist above a particular bias field. Micromagnetic simulations and Fourier imaging revealed that modes from the higher frequency branch had large amplitude at the center of the element where the effective field was parallel to the bias field and the static magnetization. Modes from the lower frequency branch had large amplitude near the edges of the element perpendicular to the bias field. The simulations revealed significant canting of the static magnetization and effective field away from the direction of the bias field in the edge regions. For the smallest element sizes and/or at low bias field values, the effective field was found to become antiparallel to the static magnetization. The simulations revealed that the majority of the modes were delocalized with finite amplitude throughout the element while the spatial character of a mode was found to correlate with the spatial variation in the total effective field and the static magnetization state. The frequencies of the edge modes are strongly affected by the spatial distribution of the static magnetization state both within the element and within its nearest neighbors.

Note also that, in the absence of translational invariance caused by the finite size of the sample, there is no requirement for conservation of momentum. However, similar to bulk samples, the suggestion of momentum conservation is conceptually useful for the nanostructured samples, as well. The fact that all spin-wave modes are standing waves implies that all modes have a total momentum of zero, i.e., each state now has both +**k** and −**k** components, so that the sum of the wave vectors for a given mode is zero [39]. As a result, the standard Gilbert damping is insufficient to describe the spin dynamics in nanomagnets.

At present, several different theoretical models attempt to explain the dependence of the resonance frequencies and damping on nanomagnet size [17,18,33,40]. On the other hand, a comparison of experimental data with theory is not so simple because an extraction of the damping parameter from measurements of ensemble nanomagnets is not a trivial task. Indeed, (i) the resonance frequencies might differ from nanomagnet to nanomagnet; (ii) shape distortions can give rise to mode splitting; (iii) the dipolar interaction between nanomagnets is nonzero, etc. Therefore, only systematic comparison of data obtained on individual nanomagnets with theory gives possibility to examine the dependence of damping on various spin-wave modes in nanomagnets of different size.

3.1. Three-magnon scattering

As already mentioned, in small elements, the wave vector becomes a set of discrete values. This limits the availability of states at the frequency of ω. As a result, localized modes become more important for nanoscale samples than usual magnetostatic waves in extended films. These modes often have low frequencies and provide a mechanism for a decay that does not involve usual magnetostatic waves. In general, in nanomagnets different nonlinear mechanisms can exist, which results in an anomalous increase in the linewidth at low frequencies. As a rule, the measured linewidth for the nanoscale magnets does not exhibit a linear dependence on frequency even at the lowest frequencies [36]. Micromagnetic simulations confirmed this behavior.

Let us illustrate some specifics in the field on an example of three-magnon damping in thin film recently discussed by Camley [39]. (For a bulk ferromagnet, such three-magnon scattering is important for the saturation of ferromagnetic resonance [22].)

Following Ref. 39, let us assume that the quantized wave vectors in the *xoy*-plane are given by $q_z = \pm n\pi / L_z$, where L_z is the length of the nanoelement in the *oz* direction and *n* is an integer. In addition, in finite systems, all the modes are essentially standing ones and contain both positive $+q_z$ and negative $-q_z$ wave-vector contributions. As a result, the conservation of energy and momentum rules are modified so that now we can have a three-magnon process where an initial spatially uniform mode ($\mathbf{k} = 0$) with a frequency ω_0 decays to two modes, one at frequency $\omega_0 / 2 + \Delta\omega$ and the other at $\omega_0 / 2 - \Delta\omega$. For this process to occur, there must be two states spaced equally (in frequency space) about $\omega_0/2$. Because the dispersion relation is no longer continuous, this can only happen at a few special points. The process also conserves momentum: the initial wave vector has k zero and the total final wave vector is zero, as each state now has both +**k** and −**k** components. This set of decay possibilities is illustrated in Fig. 3.

It is important to note that the existence of the three-magnon process depends critically on the dimensions of the nanoelement. In particular, as was shown by Camley [39], the three-magnon process, which leads in thin films to waves at ω/2, produces a different result in rectangular

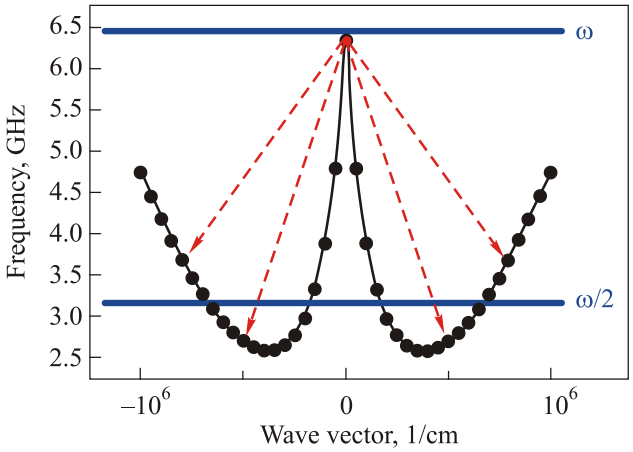

Fig. 3. (Color online) The lowest-frequency dipole-exchange mode in a nanoelement for propagation parallel to the applied field (typical Permalloy parameters used). The finite length of the sample leads to a discretization of the allowed wave vectors. The dashed lines indicate possible decays from the uniform mode ($k = 0$) to two modes equally spaced about the half-frequency position. (Borrowed from [39]).

magnetic nanoelements. This nonlinear relaxation mechanism leads to responses at several frequencies that are symmetrically spaced around ω/2. When the driving field is large and near the resonance frequency for the uniform mode, the excitation spectrum can be quite complicated. However, many of the peaks seen in that spectrum result from nonlinear combinations of the original wave.

3.2. Longitudinal relaxation

Both the Landau–Lifshitz and the Gilbert phenomenological damping terms suggested that the magnetic losses could be characterized by a single intrinsic damping constant of relativistic nature. As stressed in Introduction, within the LL (LLG) damping term's structure the length of |M| stays constant while the projection of the magnetization onto the *z*-axis, M_z, increases as it relaxes to its equilibrium position and the angle between vectors $\mathbf{H}_{\text{eff}}$ and $\mathbf{M}$ decreases. In magnetic nanoelements the internal magnetic field is strongly inhomogeneous and one can suggest a relaxation mechanism when the projection of M_z stays constant but the precessional energy is dissipated into the transverse magnetization components, i.e., a local reduction of the magnetization length and longitudinal relaxation. Naturally, the question arises whether there is any experimental evidence supporting this suggestion. The answer is positive. Recent experiments [25,41] and theories [39,42] point out that *even at low temperature* there is no reason to assume a fixed magnetization length for magnetic nanoelements. In particular, the uniform motion of the magnetization may scatter into excited states of the magnetic subsystem — magnetic thermal bath (spin waves, Stoner excitations, etc.). Respectively, the projection of $\mathbf{M}$ onto the *z*-axis stays constant but |M| is decreased since the precessional energy is scattered into the transverse components M_x and M_y. This is another example proving that the phenomenological Gilbert (as well as the Landau–Lifshitz) damping parameter cannot correctly describe the magnetic relaxation in magnetic nanostructures.

Investigation of longitudinal relaxation mechanisms is a very challenging problem, which has recently received new impulse in connection with ultrafast remagnetization (see reviews [19,20]). Within the goal of this report, the purpose is to search the longitudinal relaxation channels in small magnetic elements in relation with their geometric characteristics and micromagnetic configuration. Note that this interesting scientific direction is just emerging.

As both relaxation mechanisms (longitudinal and transverse) can be active in nanostructures, the questions arise how to include longitudinal relaxation into description and how to separate experimentally the scattering to nonmagnetic degrees of freedom (direct damping) from the dissipative relaxation to the magnetic thermal bath (longitudinal relaxation). One of the theoretical backgrounds to study this question was been known for a long time. We mean the Bloch–Bloembergen equation written as follows

$$\partial\mathbf{M}/\partial t = -\gamma_G \mathbf{M}\times\mathbf{H}_{\text{eff}} - \frac{M_x\mathbf{e}_x + M_y\mathbf{e}_y}{T_2} - \frac{M_z - M_s}{T_1}\mathbf{e}_z. \quad (9)$$

Indeed, in this case two different relaxation times are introduced into the magnetization dynamics: the longitudinal relaxation time T_1 for the component of the magnetization parallel to the field $\mathbf{H}_{\text{eff}}$, i.e., the direct path into the thermal bath, and the so-called transverse time, T_2, by which energy is scattered into the transverse magnetization components M_x and M_y. Analysis of the ferromagnetic resonance in nanostructures within the framework of Eq. (9) is performed in Ref. 41.

Here we briefly outline a possible alternative formalism, which is based on generalization of the damping term proposed by Bar'yakhtar [4].

The general form of the LL–Bar'yakhtar equation (LLBar) reads:

$$\partial\mathbf{M}/\partial t = -\gamma\mathbf{M}\times\mathbf{H}_{\text{eff}} + \hat{\lambda}(\mathbf{M})\mathbf{H}_{\text{eff}} - \hat{\lambda}^{(e)}_{ij}(\mathbf{M})\frac{\partial\mathbf{H}_{\text{eff}}}{\partial x_i \partial x_j}. \quad (10)$$

As usual, the first term in the r.h.s. defines the precession of the vector $\mathbf{M}$ in effective field $\mathbf{H}_{\text{eff}}$, while the second and the third terms describe the local and *nonlocal* relaxations, respectively. Here $\hat{\lambda}(\mathbf{M})$ and $\hat{\lambda}^{(e)}_{ij}(\mathbf{M})$ are the relaxation tensors of relativistic and exchange nature, respectively, and in general are functions of the magnetization vector. These tensors describe how crystallographic and magnetic symmetries of the system manifest themselves into the relaxation mechanisms of magnetic subsystem.

It is important to note that, even in a local approximation, i.e., keeping only the second term in the r.h.s. of Eq. (10), the Bar'yakhtar equation, in contrast to the Lan-

dau–Lifshitz formalism, does not conserve the length of the magnetization vector and $|\mathbf{M}| \neq$ const. For simplicity, we focus here on the intermediate range of temperature, when it is reasonable to expect that relativistic effect cannot compete with the exchange force that tries to keep the magnetization vector length constant and variations of the magnetization vector length cannot significantly contribute to the magnon-magnon scattering and, thereby, to the FMR linewidth broadening. The dynamic contribution of the nonlocal damping becomes significant only when the wavelength of magnons approaches the exchange length of the material. Therefore, both static and dynamic contributions of the nonlocal damping are vanishing, and Eq. (10) can be written as:

$$\partial \mathbf{M} / \partial t = -\gamma \mathbf{M} \times \mathbf{H}_{\text{eff}} - \gamma M_s \hat{\alpha} \mathbf{H}_{\text{eff}} \ . \qquad (11)$$

Here, again for simplicity, expanding the relaxation tensor, we keep only the coefficients of the expansion that take into account crystallographic symmetry and write $\hat{\lambda}(\mathbf{M}) \approx \hat{\lambda}(0) = -\gamma M_s \hat{\alpha}$. Note that, in spite of its relatively simple form, Eq. (11) still includes a contribution due to the exchange energy arising from changes of the magnetization vector length, i.e., does not conserve the length of the magnetization vector. Indeed, by representing $\mathbf{M}$ as $\mathbf{M} = M\mathbf{m}$, where $\mathbf{m}$ is the unit vector, and substituting this in Eq. (11), after simple algebra one can obtained a system of two coupled equations [42]:

$$\partial \mathbf{m} / \partial t = -\gamma \mathbf{m} \times \mathbf{H}_{\text{eff}} - \gamma \frac{M_s}{M} [\mathbf{m} \times \hat{\alpha} (\mathbf{m} \times \mathbf{H}_{\text{eff}})],$$

$$\partial M / \partial t = \gamma M_s \mathbf{m} \hat{\alpha} \mathbf{H}_{\text{eff}} .$$

Thus, Eq. (11) describes nonconservative magnetization dynamics.

Concerning the experiment, it was demonstrated [25,41], that both angular and frequency dependent measurements of the linewidth give a direct possibility to distinguish the transverse scattering rate within the magnetic subsystem and the longitudinal relaxation into the thermal bath. For the particular system investigated in [25], Fe/V multilayers, the longitudinal relaxation scattering was about two orders of magnitude faster than transverse (Gilbert) damping.

A number of magnetic resonance experiments have been performed by various authors on assemblies of randomly oriented nanoparticles (see, e.g., [43] and references therein). The agreement between experimental data and theoretical predictions is, however, rather poor and does not allow for accurate quantitative analysis of the experimental results. The only exception is the high-temperature limit where, according to the conventional theory, the spectrum progressively collapses into a single nearly Lorentzian line. At lower temperatures, significant broadening of the single line was found together with its progressive shifting to lower fields with cooling. We note here the report of Noginova *et al.* [44], where the magnetization dynamics of γ-Fe_2O_3 nanoparticles has been studied by electron magnetic resonance (EMR) at 77–380 K and an original model of the longitudinal spin relaxation was proposed. In this report, slightly asymmetric spectra observed at room temperature become much broader and symmetric, and shift to lower fields upon cooling. The longitudinal relaxation time, $T_1 \approx 10$ ns, was determined by a specially developed modulation method. The shift and broadening of the spectrum upon cooling were assigned to the effect of the surface-related anisotropy. To describe the overall spectral shape, the original "quantization" model was used which includes summation of resonance transitions over the whole energy spectrum of a nanoparticle considered as a giant exchange cluster. This approach, supplemented with some phenomenological assumptions, provides satisfactory agreement with the experimental data.

Yet, as already noted, such interesting scientific area as longitudinal magnetization relaxation in small-scale magnetic objects is just at its beginning. Further work in theory and experiment is needed to overcome our very little understanding in this field.

3.3. Anisotropic damping in nanoelements

We briefly discuss anisotropic damping in nanoscale samples based on recent theoretical analysis made in Ref. 42. This analysis utilizes the Bar'yakhtar generalization of the damping term, namely, Eq. (11). The simulations were carried out for a thin magnetic disk and an ellipse.

The dominant peaks in the spectra (attributed to the magnonic resonances of different spatial characters) are fitted to Lorentzian curves in order to extract their amplitudes, frequencies ω, and full width at half-maximum $\Delta\omega$. The latter two parameters are used to estimate the relative net relaxation rates given by the LLBar model as $\Gamma_{LLBar} = \Delta\omega_{LLBar} / \omega_{LLBar}$. The angular dependence of Γ_{LLBar} is calculated for the edge mode for an isotropic disk and an ellipse. For the disk, the symmetry of Γ_{LLBar} was found to be either isotropic or twofold for an out-of-plane and in-plane reduction of the relaxation tensor, respectively. In contrast, for the ellipse the symmetry is always twofold, even for the case when the tensor is altered out of plane and, thereby, homogeneous in plane. Therefore, the shape anisotropy also contributes to the symmetry of the relative relaxation rate. This is also supported by the fact that the relative relaxation rates are different for in-plane and out-of-plane reductions of the relaxation tensor, i.e., along easy and hard axes, respectively.

In total, the results obtained in an isotropic disk and an ellipse are threefold [42]. First, the highest reduction of relative relaxation rate is observed when the shortest eigenvector of the relaxation tensor is parallel to the hardest degree of freedom. Second, the reduction (enhancement) of characteristic frequency leads to the reduction (enhancement) of the contribution of the corresponding relaxation

channel. Third, the authors [42] showed that the symmetry of the magnonic relative relaxation rate with respect to the direction of saturation is determined by the superposition of the symmetries of the relaxation tensor and the ellipse of motion. The latter is mode-specific due to the competition between the shape anisotropy and the exchange energy (that eventually becomes dominant for high-order magnons), thereby making the absolute value of the relative relaxation rate frequency dependent.

These conclusions could be used to design a test experiment, e.g., measurements of the magnonic linewidths in nanoelements with in-plane and out-of-plane uniaxial anisotropies. Then by estimating the characteristic frequencies from the micromagnetic simulations, the corresponding components of the relaxation tensor could be extracted. An angular dependence of magnetic losses (or effects associated with the same physics) has already been observed experimentally [45–49].

4. Nanometre-scale patterned magnetic structures

Patterned magnetic media have attracted a lot of attention recently due to both fundamental and technological interest. High-quality nanopatterned magnetic structures can be a 2D magnonic crystal [50–52], the basis for magnetic metamaterials [53], and offers new ways for the development of data processing without moving electrical charges with working frequencies in the GHz range [7,54,55]. Fundamentally, the question of how nanosized non-magnetic inclusions affect macroscopic and microscopic magnetic properties of continuous thin film is of great interest. Particularly, the switching mechanism of patterned magnets during the magnetization reversal process is among the important issues that are not well understood in the nanoscale regime yet. When the desired response time is in the GHz range, the switching behavior of magnetic elements is determined by the FMR frequencies and the corresponding damping times. However, the patterning leads to less uniform and more complex magnetization dynamics that has not yet received exhaustive explanation even on a phenomenological level.

We illustrate some specifics in this field on an example of a thin film with mesh of holes (antidots). The effect of holes size and lattice parameters on magnetization dynamics has been studied in Refs. 56–61. It was shown that magnetic antidots enable to induce a configurational anisotropy. Its value is determined by the symmetry of the lattice, size and shape of the holes, and can be controlled during sample preparation [62]. The extra broadening of resonance line is also detected. Let us imagine the antidot lattice as a two-dimensional network of interconnected magnetic nanowires. Then it is reasonable to expect anisotropy effects of spin wave propagation, as well. Indeed, it was observed [63] that, depending on the orientation of the external field, spin waves propagate at velocities being comparable with or a factor of about two smaller than the velocities found for a continuous film. The damping characteristics were also highly anisotropic suggesting that extrinsic damping, e.g., due to edge-roughness mediated scattering, is relevant in an antidot lattice. A deep understanding of the respective parameters is important for fundamental research. Naturally, all these features are very critical for applications.

4.1. FMR damping

In a film with nonmagnetic inclusions (e.g., holes), in addition to the intrinsic damping inherent to the particular material, one can also expect specific relaxation channels due to the film's patterned structure. However, the investigation of relaxation mechanisms in relation to the geometric parameters and micromagnetic configuration of a patterned structure is a challenging problem that has received a little attention up to date. We note here the report by Martyanov *et al.* [64], where measurements were performed on geometrically scaled antidot arrays with a rectangular unit cell. (In Ref. 64 two samples with different periods, but with a fixed ratio of the hole's radius, r, to the lattice period, a, were studied.) The authors found a strong attenuation of the uniform FMR mode compared to the resonance mode of a continuous film and attributed the broadening to a two-magnon process, which scatters energy from the uniform mode to other degenerate modes with higher wave numbers.

The authors [60,61,65] used micromagnetic simulations and a semianalytical approach to model the FMR dependence on geometrical parameters of the antidot lattice. The approach used directly accounts for the effects of the magnetic state nonuniformity, allows avoiding a numerical calculation on the step of restoring a system's linear dynamic properties, and offers physical transparency for what is usually hidden behind numerical micromagnetic simulations. An example of micromagnetic modeling of static magnetic configuration of the hexagonal antidot lattice in external magnetic field normal to the film plane is shown in Fig. 4(a). The domain structure obtained consists of three regions with different magnetization orientation in the magnetic unit cell. In two of them, regions *A* and *B* in Fig. 4(a), a direction of magnetic moments differs from the direction of spontaneous magnetization. In the third area, region *C* in Fig. 4(a), the magnetic moments are parallel to the unit cell total magnetization. Since the external field is oriented perpendicular to film plane, i.e., symmetry of the magnetic system is not broken, the projection of the spontaneous magnetization on the film plane is directed along one of the "easy" axes, which coincides with the short diagonal of the unit cell of a hexagonal lattice of antidots. (For the case shown in Fig. 4(a) this is a direction along the arrow in the upper left corner, angle $\alpha = 60°$ to the *ox*-axis.) While the "hard" axis is the direction along the long diagonal of the cell.

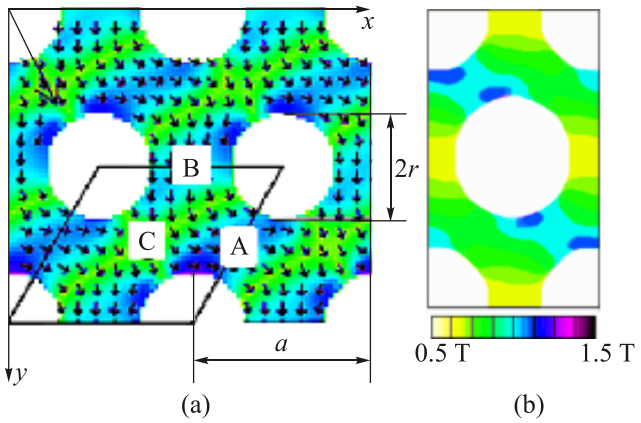

Fig. 4. (Color online) Domain structure of hexagonal antidote lattice r/a = 0.3 in Permalloy film. The grayscale shows the local magnetization deviation from the direction of unit cell total magnetization (a). Resonance frequencies distribution on antidot lattice cell H = 0.7T, r/a = 0.35, h = 10 nm. Angle between anisotropy axes and field direction is 78° (b). (Borrowed from [65]).

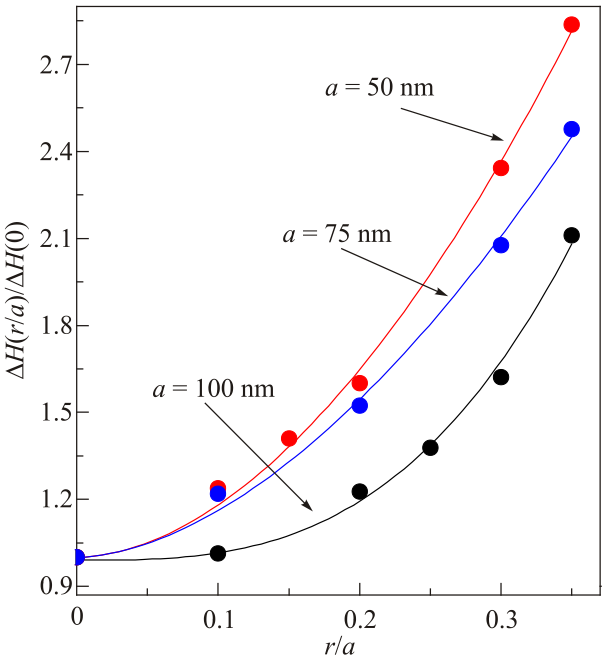

Fig. 5. (Color online) The dependence of the FMR linewidth ΔH, as function of the geometrical factor r/a for hexagonal antidot lattice with different lattice period a (Borrowed from [60]).

The calculation of local dynamic susceptibility tensor yields that the resonance spectra consist of three different quasi-uniform modes of magnetization precession related to the precession of the magnetic moment in the regions *A*, *B* and *C*. An example of resonance frequencies distribution within a unit cell is shown in Fig. 4(b). Each of the resonant modes follows a two-fold variation with respect to the in-plane orientation of the applied magnetic field. The easy axes of the modes are mutually rotated by 60 degrees and combine to yield an apparent six-fold configurational anisotropy.

Figure 5 summarizes the revealed theoretical dependences of the total FMR linewidth, ΔH, in the hexagonal magnetic antidot lattice as a function of the geometrical factor (r/a) for structures with different lattice periods a (the damping parameter α is fixed). It is apparent that the width of the FMR line increases with an increase of magnetic inhomogeneity (i.e., with an increase of the density of holes). The dependence for the FMR linewidth on the parameter (r/a) as compared to a continuous film could be reasonably fitted by a scaling form

$$[\Delta H(r/a) - \Delta H(0)]/\Delta H(0) \sim (r/a)^{\eta}.$$

The critical exponent η is function of the lattice period (η = 2.22, 2.30, and 3.33 for structures with lattice period a = 50,75, and 100 nm, respectively).

Another important parameter here is a film thickness. The variation of the film thickness leads to changes in anisotropic properties of the system, too. With increasing film thickness, there is not only an increase of the induced anisotropy (a magnitude of resonance frequency angular dependence), but also a shift of the spectrum minimum to lower frequencies. In addition, with increasing film thickness, a multiple resonance structure becomes more pronounced in spite of larger resonance line-width. In accordance with theoretical predictions, the experimental data of FMR spectra [65] of the antidot lattices for film thicknesses 10 nm and 25 nm indeed contain only three modes, which are well fitted by three quasi-uniform modes of magnetization precession. For thicker films, three resonance modes are clearly observed for the in-plane field geometry and additional (spin-wave) modes are detected in the normal-to-plane geometry. As it expected, the inhomogeneous distribution of magnetization and the effective field in antidot lattices lead to substantial differences in the forms of spin-wave lines and the resonant fields for the film with antidot lattice and homogeneous film [65].

4.2. Spin waves anisotropic propagation and damping

The antidot lattice, if considered as a two-dimensional network of interconnected magnetic nanowires, is a relevant model system to study the possible anisotropy effects of spin wave propagation. Such effects were recently studied by time-resolved magneto-optical Kerr microscopy [63].

The permalloy film was periodically patterned into a square lattice. The holes (diameter of 120 nm) are arranged on a square lattice with a period of 800 nm. For the continuous film, one obtains a relaxation time of 0.6 ns, which does not depend on propagation angle φ. For the antidot lattice the authors [63] observed angle-dependent relaxation characteristics. At regime *A* (φ = 0°, f = 8 GHz, $\mu_0 H$ = = 68 mT) the effective relaxation time is 0.70 ns, and was comparable with the plain film. A minimum relaxation time of 0.37 ns is found at regime *B* (φ = 22°, f = 5.2 GHz, $\mu_0 H$ = 20 mT). If compared to regime *A*, the effective relaxation increases by a factor of almost two. A larger re-

laxation time, 0.49 ns, is regained at regime *C* (φ = 30°, f = 8 GHz, $\mu_0 H$ = 75 mT) but still the value is smaller than that of at φ = 0° and of the continuous film. The relaxation times vary with the characteristic mode profiles illustrated in Fig. 6(a)–(c). In regime *B* the propagating mode has a higher oscillation amplitude near the edges of the holes if compared to *A* and *C* regimes. Near the hole edges, the internal field can vary due to edge roughness and possible reduced saturation magnetization. Via magnon-magnon scattering, such irregularities can open further relaxation channels. This might explain the anisotropy of damping found in the angular dependent experiments. However, a theory linking mode profiles and edge roughness with relaxation is missing.

These results show that by removing only a small fraction of material from a film to form an antidot lattice, the properties of propagating spin waves are significantly altered. Depending on the orientation of the external field, spin waves can propagate at velocities being comparable with or a factor of about two smaller than for a plain film. In contrast to the film, the damping characteristics turn out to be highly anisotropic suggesting that extrinsic damping due to, e.g., edge-roughness mediated scattering is relevant in an antidot lattice. The dependence of the damping on the orientation of **M** represents an additional option to optimize a magnetization reversal process in a nanostructured system by choosing a magnetization trajectory which is most appropriate from the viewpoint of damping.

Spin-wave modes in thin-film antidot lattices are investigated theoretically in Ref. 66 using micromagnetic simulations and a semianalytical theoretical approach. The simulations reveal a rich eigenmode spectrum consisting of edge and center modes. Both spatially localized and spin waves were found to be extending over many unit cells. For lattices of unit-cell lengths ranging from 200 to 1100 nm, the authors found that the characteristic mode eigenfrequencies could be correlated with both local inhomogeneities of the demagnetization field and specific wave vectors caused by geometry-imposed mode quantization conditions.

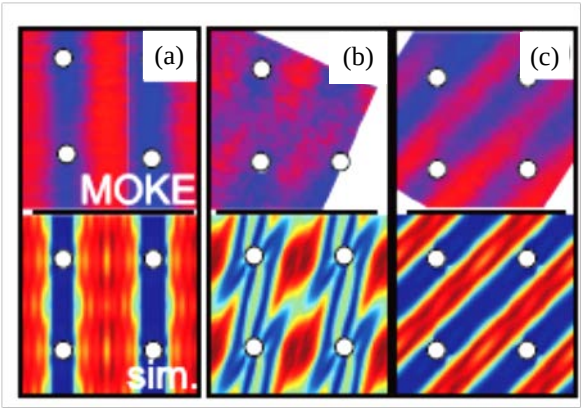

Fig. 6. (Color online). (a)–(c) Spatial spin-wave mode profiles obtained by time-resolved magneto-optical Kerr microscopy (upper row). Shown are modes in the three different regimes: (a) $A - \varphi = 0°$, f = 8 GHz, $\mu_0 H$ = 68 mT, (b) $B - \varphi = 25°$, $f = 5{:}2$ GHz, $\mu_0 H$ = 20 mT, and (c) $C - \varphi = 30°$, f = 8 GHz, $\mu_0 H$ = 75 mT. Simulation data (lower row) are obtained at $\mu_0 H$ = 20 mT and, in particular, **k** = 0. The eigenfrequencies are (a) 3.8 GHz, (b) 4.3 GHz, and (c) 3.9 GHz. Bright (dark) contrast reflects high (low) spin-precession amplitude. (Borrowed from [63]).

In conclusion of this section, note that the recent progress in simulations of the excitation and propagation, and other wave characteristics of spin waves, in nanometre-scale patterned magnetic elements can be found in review paper [67]. Many examples of micromagnetic modelling for numerical calculations, employing various dimensions and shapes of patterned magnetic elements, are given here, too. The current limitations of continuum micromagnetic modelling and of simulations based on the LLG equation of motion of magnetization are also discussed, along with further research directions for spin-wave studies.

5. Conclusion

The high-frequency excitations in confined magnetic structures exhibiting nonuniform magnetization distributions are the subject of a growing interest at present. In addition to interest from the fundamental physics point of view, there are practical reasons for this. The purpose is to investigate and then to control (to reduce/enhance) the relaxation channels in such systems in relation with their geometric characteristics and magnetic structure. Naturally, in this connection, the question was raised whether the LL (LLG) phenomenological damping parameter is applicable to magnetic nanomagnetic elements and nanostructured samples. Based on the results of recent advanced experiments and theoretical analysis the answer is “No”. Analysis within the Bar’yakhtar generalization of the damping term [42] inspires hopes that this approach can be a reasonable phenomenology, which can provide us with a realistic description of spin motions in ultrathin ferromagnet films and in large number of magnetic nanostructures. Yet, further work is definitely needed to prove this expectation. In addition, it should be taken into account that all results based on a phenomenological approximation are valid for time scales longer than the picosecond and dimensions greater than the nanometre. Phenomena associated with faster-dynamics and atomic spatial resolution require microscopic consideration.

The absence of fruitful microscopic theory, which is able to give true recommendation to control the relaxation, is one of the reasons why nanomagnonic devices realized so far suffer from the relatively short damping length. However, there are reasons to expect that situation can be drastically change in the nearest future. Very recent experimental publications demonstrate that the ultra-thin-film ferrimagnet insulator YIG (yttrium iron garnet) allows

overcoming the damping problem for nanomagnetism and to boost further developments in nanomagnonic devices technology for processing at GHz operational frequencies. Liu *et al.* [68] studied ferromagnetic resonance of YIG films with a thickness of 7 to 26 nm finding a promising damping constant of 0.001. This value is already a factor of about three better than the metallic ferromagnets used in magnonics. Hahn *et al.* showed that the damping constant is unaffected when nanostructuring ultra-thin YIG films [69]. Pirro *et al.* [70] studied a 100 nm thick YIG thin film and observed a spin-wave decay length of 31 μm. Unprecedented results for now were obtained in Ref. 71. Authors demonstrate that in nm-thick YIG films propagating spin waves can exhibit a damping parameter of $2.3\ 10^{-4}$. Estimated macroscopic of damping length value was of about one mm allowing for magnonics-based nanotechnology with ultra-low damping. The spin wave group velocities are found to vary between 0.6 km/s and 1.2 km/s depending on the wave vector and applied magnetic field. This experimental work demonstrates that the thin-film ferrimagnet insulator YIG allows overcoming the damping problem for nanomagnetism and boosting further developments in nanomagnonic devices technology for processing at GHz operational frequencies. These results definitely motivate further fundamental investigation in the field.

Numerous fruitful discussions with S.M. Ryabchenko are gratefully acknowledged. The author would like to thank V.O. Golub for critical reading of the manuscript. This work was partly supported from the European Union's Horizon 2020 research and innovation programme under the Marie Skłodowska-Curie grant agreement No 644348 (MagIC).

1. L. Landau and E. Lifshitz, *Phys. Z. Sowjetunion* **8**, 153 (1935).
2. T.L. Gilbert, *Phys. Rev.* **100**, 1243 (1955); T.L. Gilbert and J.M. Kelly, *Conference on Magnetism and Magnetic Materials*, Pittsburgh, PA, 14–16 June, 1955, American Institute of Electrical Engineers, NewYork (1955), p. 253.
3. H.B. Callen, *J. Phys. Chem. Solids* **4**, 256 (1958).
4. V.G. Bar'yakhtar, *Sov. Phys. JETP* **60**, 863 (1984); *Phys. B Condens. Matter* **159**, 20 (1998); V.G. Bar'yakhtar and A.G. Danilevich, *Fiz. Nizk. Temp.* **36**, 385 (2010) [*Low Temp. Phys.* **36**, 303 (2010)]; *ibid*. **39**, 1278 [993] (2013).
5. V.G. Bar'yakhtar, B.A. Ivanov, V.N. Krivoruchko, and A.G. Danilevich, *Modern Problems of Magnetization Dynamics: from the Basis to Ultrafast Relaxation*, Kiev, Himgest, (2013) (in Russian).
6. B.D. Terris and T. Thomson, *J. Phys. D: Appl. Phys.* **38**, *R* 199 (2005).
7. V.V. Kruglyak, S.O. Demokritov, and D. Grundler, *J. Phys. D: Appl. Phys.* **43**, 264001 (2010); A.A. Serga, A.V. Chumak, and B, Hillebrands, *J. Phys. D: Appl. Phys*. **43**, 264002 (2010).
8. K.-S. Lee, D.-S. Han, and S.-K. Kim, *Phys. Rev. Lett.* **102**, 127202 (2009).
9. *Magnonics: From Fundamentals to Applications* (*Topics in Applied Physics*), S.O. Demokritov and A.N. Slavin, (Eds.), Springer, (2013).
10. Y. Tserkovnyak, A. Brataas, G.E.W. Bauer, and B.I. Halperin, *Rev. Mod. Phys.* **77**, 1375 (2005).
11. J.C. Slonczewski, *J. Magn. Magn. Mater*. **159**, L 1 (1996).
12. L. Berger, *Phys. Rev. B* **54**, 9353 (1996).
13. Y. Tserkovnyak, A. Brataas, and G.E.W. Bauer, *Phys. Rev. Lett.* **88**, 117601 (2002).
14. E.B. Myers, D.C. Ralph, J.A. Katine, R.N. Louie, and R.A. Buhrman, *Science* **285**, 867 (1999); C.H. Back, R. Allenspach, W. Weber, S.S.P. Parkin, D. Weller, E.L. Garwin, and H.C. Siegmann, *Science* **285**, 864 (1999).
15. J.A. Katine, F.J. Albert, R.A. Buhrman, E.B. Myers, and D.C. Ralph, *Phys. Rev. Lett.* **84**, 3149 (2000); F. Schreiber, J. Pflaum, Z. Frait, T. Mühge, and J. Pelzl, *Solid State Commun.* **93**, 965 (1995).
16. H.M. Olson, P. Krivosik, K. Srinivasan, and C.E. Patton, *J. Appl. Phys.* **102**, 023904 (2007).
17. J.M. Shaw, T.J. Silva, M, L. Schneider, and R.D. McMichael, *Phys. Rev. B* **79**, 184404 (2009).
18. H.T. Nembach, J.M. Shaw, C.T. Boone, and T.J. Silva, *Phys. Rev. Lett.* **110**, 117201 (2013).
19. A. Kirilyuk, A. Kimel, and T. Rasing, *Rev. Mod. Phys.* **82**, 2731 (2010).
20. B.A. Ivanov, *Fiz. Nizk. Temp.* **40**, 119 (2014) [*Low Temp. Phys.* **40**, 91 (2014)].
21. M.M. Krupa, *SPIN* **4**, 1450006 (2014).
22. A.G. Gurevich and G.A. Melkov, *Magnetization Oscillations and Waves*, CRC Press, Boca Raton, FL (1996).
23. R. Arias and D.L. Mills, *Phys. Rev. B* **60**, 7395 (1999); R. Arias and D.L. Mills, *J. Appl. Phys.* **87**, 5455(2000); D.L. Mills and R. Arias, *Physica B* **384**, 147 (2006).
24. M. Sparks, R. Loudon, and C. Kittel, *Phys. Rev.* **122**, 791 (1961).
25. R. Urban, B. Heinrich, G. Woltersdorf, K. Ajdari, K. Myrtle, J.F.Cochran, and E. Rozenberg, *Phys. Rev. B* **65**, 020402 (2001); K. Lenz, H. Wende, W. Kuch, K. Baberschke, K. Nagy, and A. Jánossy, *Phys. Rev. B* **73**, 144424 (2006).
26. I. Barsukov, F.M. Römer, R. Meckenstock, K. Lenz, J. Lindner, S. Hemken to Krax, A. Banholzer, M. Körner, J. Grebing, J. Fassbender, and M. Farle, *Phys. Rev. B* **84**, 140410(R) (2011).
27. V.V. Kruglyak and A.N. Kuchko, *Phys. Met. Metallogr.* **92**, 211 (2001); *ibid*. **93**, 511 (2002); *J. Magn. Magn. Mater*. **302**–**303**, 272 (2004).
28. S.M. Rezende, A. Azevedo, M.A. Lucena, and F.M. Aquiar, *Phys. Rev. B* **63**, 214418 (2001).
29. W. Stoecklein, S.S.P. Parkin, and J.C. Scott, *Phys. Rev. B* **38**, 6847 (1988); R.M. McMichael, M.D. Stiles, P.J. Chen, and W.F. Egelhoff, Jr., *J. Appl. Phys.* **83**, 7037 (1998).
30. T. Bose and S. Trimper, *Phys. Rev. B* **85**, 214412 (2012).
31. V.G. Bar'yakhtar, *Fiz. Nizk. Temp.* **40**, 804 (2014) [*Low Temp. Phys.* **40**, 626 (2014)].
32. C. Le Graët, D. Spenato, S.P. Pogossian, D.T. Dekadjevi, and J. Ben Youssef, *Phys. Rev. B* **82**, 100415(R) (2010).

33. D. Steiauf and M. Fähnle, *Phys. Rev. B* **72**, 064450 (2005).
34. V.L. Safonov, *J. Appl. Phys.* **91**, 8653 (2002).
35. S.D. Bader, *Rev. Mod. Phys.* **78**, 1 (2006).
36. R.D. McMichael, D.J. Twisselmann, and A. Kunz, *Phys. Rev. Lett.* **90**, 227601 (2003).
37. J. Jorzick, S.O. Demokritov, B. Hillebrands, M. Bailleul, C. Fermon, K.Y. Guslienko, A.N. Slavin, D.V. Berkov, and N.L. Gorn, *Phys. Rev. Lett.* **88**, 047204 (2002); K.Yu. Guslienko, and A.N. Slavin, *Phys. Rev. B* **72**, 014463 (2005).
38. P.S. Keatley, V.V. Kruglyak, A. Neudert, E.A. Galaktionov, R.J. Hicken, J.R. Childress, and J.A. Katine, *Phys. Rev. B* **78**, 214412 (2008).
39. R.E. Camley, *Phys. Rev. B* **89**, 214402 (2014).
40. R.D. McMichael and B.B. Maranville, *Phys. Rev. B* **74**, 024424 (2006).
41. K. Baberschke, *Phys. Status Solidi B* **245**, 174 (2008); K. Baberschke, *J. Physics: Conference Series* **324**, 012011 (2011).
42. M. Dvornik, A. Vansteenkiste, and B. van Waeyenberge, *Phys. Rev. B* **88**, 054427 (2013).
43. R. Berger, J. Kliava, J.-C. Bissey, and V. Baïetto, *J. Appl. Phys.* **87**, 7389 (2000); Yu.A. Koksharov, D.A. Pankratov, S.P. Gubin, I.D. Kossobudsky, M. Beltran, Y. Khodorkovsky, and A.M. Tishin, *J. Appl. Phys.* **89**, 2293 (2001); V.V. Pishko, S.L. Gnatchenko, V.V. Tsapenko, R.H. Kodama, and S.A. Makhlouf, *J. Appl. Phys.* **93**, 7382 (2003); V.N. Krivoruchko, A.I. Marchenko, and A.A. Prokhorov, *Fiz. Nizk. Temp.* **33**, 578 (2007) [*Low Temp. Phys.* **33**, 433 (2007)].
44. N. Noginova, F. Chen, T. Weaver, E.P. Giannelis, A.B. Bourlinos, and V.A. Atsarkin, *J. Phys.: Condens. Matter*. **19**, 246208 (2007).
45. P.S. Keatley, P. Gangmei, M. Dvornik, R.J. Hicken, J.R. Childress, and J.A. Katine, *Appl. Phys. Lett.* **98**, 082506 (2011).
46. H.W. Schumacher, S. Serrano-Guisan, K. Rott, and G. Reiss, *Appl. Phys. Lett.* **90**, 042504 (2007); S. Serrano-Guisan, K. Rott, G. Reiss, and H.W. Schumacher, *J. Phys. D* **41**, 164015 (2008).
47. S. Mizukami, Y. Ando, and T.Miyazaki, *Jpn. J. Appl. Phys.* **40**, 580 (2000).
48. M.L. Schneider, J.M. Shaw, A.B. Kos, T. Gerrits, T.J. Silva, and R.D. McMichael, *J. Appl. Phys.* **102**, 103909 (2007).
49. M. Buchmeier, D.E. Bürgler, P.A. Grünberg, C.M. Schneider, R. Meijers, R. Calarco, C. Raeder, and M. Farle, *Phys. Status Solidi A* **203**, 1567 (2006).
50. S.A. Nikitov, P. Tailhades, and C.S. Tsai, *J. Magn. Magn. Mater*. **236**, 320 (2001).
51. M. Kostylev, G. Gubbiotti, G. Carlotti, G. Tacchi, C. Wang, N. Sing, A.O. Adeyeye, and R.L. Stamps, *J. Appl. Phys.* **103**, 07C 507 (2008).
52. S. Neusser, G. Duerr, S. Tacchi, M. Madami, M.L. Sokolovskyy, G. Gubbiotti, M. Krawczyk, and D. Grundler, *Phys. Rev. B* **84**, 094454 (2011).
53. S. Neusser and D. Grundler, *Adv. Mater.* **21**, 2927 (2009).
54. A. Khitun, M. Bao, and K.L. Wang, *J. Phys. D* **43**, 264005 (2010).
55. J.W. Lau and J.M. Shaw, *J. Phys. D* **44**, 303001 (2011).
56. G.N. Kakazei, P.E. Wigen, K.Yu. Guslienko, R.W. Chantrell, N.A. Lesnik, V. Metlushko, H. Shima, K. Fukamichi, Y. Otani, and V. Novosad, *J. Appl. Phys.* **93**, 8418 (2003).
57. S. Neusser, B. Botters, M. Becherer, D. Schmitt-Landsiedel, and D. Grundler, *Appl. Phys. Lett.* **93**, 122501 (2008).
58. D.H.Y. Tse, S.J. Steinmuller, T. Trypiniotis, D. Anderson, G.A.C. Jones, J.A.C. Bland, and C.H.W. Barnes, *Phys. Rev. B* **79**, 054426 (2009).
59. S. Martens, O. Albrecht, K. Nielsch, and D. Gorlitz, *J. Appl. Phys.* **105**, 07C 113 (2009).
60. V.N. Krivoruchko and A.I. Marchenko, *J. Appl.* **109**, 083912 (2011).
61. V.N. Krivoruchko and A.I. Marchenko, *Fiz. Nizk. Temp*. **38**, 195 (2012) [*Low Temp. Phys.* **38**, 157 (2012)]; *J. Magn. Magn. Mater*. **324**, 3087 (2012).
62. C. Castán-Guerrero, J. Herrero-Albillos, J. Bartolomé, F. Bartolomé, L.A. Rodríguez, C. Magén, F. Kronast, P. Gawronski, O. Chubykalo-Fesenko, K.J. Merazzo, P. Vavassori, P. Strichovanec, J. Ses'e, and L.M. García, *Phys. Rev. B* **89**, 144405 (2014).
63. S. Neusser, G. Duerr, H.G. Bauer, S. Tacchi, M. Madami, G. Woltersdorf, G. Gubbiotti, C.H. Back, and D. Grundler, *Phys. Rev. Lett.* **105**, 067208 (2010).
64. O.N. Martyanov, V.F. Yudanov, R.N. Lee, S.A. Nepijko, H.J. Elmers, R. Hentel, C.M. Schneider, and G. Schönhense, *Phys. Rev. B* **75**, 174429 (2007).
65. A. Vovk, V. Golub, L. Malkinski, V.N. Krivoruchko, and A.I. Marchenko, *J. Appl. Phys.* **117**, 073903 (2015).
66. S. Neusser, B. Botters, and D. Grundler, *Phys. Rev. B* **78**, 054406 (2008).
67. Sang-Koog Kim, *J. Phys. D* **43**, 264004 (2010).
68. T. Liu, H. Chang, V. Vlaminck, Y. Sun, M. Kabatek, A. Hoffmann, L. Deng, and M. Wu, *J. Appl. Phys.* **115**, 17A 501 (2014).
69. C. Hahn, V.V. Naletov, G. de Loubens, O. Klein, O. d'Allivy Kelly, A. Anane, R. Bernard, E. Jacquet, P. Bortolotti, V. Cros, J.L. Prieto, and M. Muñoz, *Appl. Phys. Lett.* **104**, 152410 (2014).
70. P. Pirro, T. Brächer, A.V. Chumak, B. Lägel, C. Dubs, O. Surzhenko, P. Görnert, B. Leven, and B. Hillebrands, *Appl. Phys. Lett.* **104**, 012402 (2014).
71. Yu. Haiming, O. d'Allivy Kelly, V. Cros, R. Bernard, P. Bortolotti, A. Anane, F. Brandl, R. Huber, I. Stasinopoulos, and D. Grundler, *Sci. Rep*. **4**, 6848 (2014).